3D STOKES-CORRELOMETRY OF THE POLYCRYSTALLINE STRUCTURE OF BIOLOGICAL TISSUES

A.Bodnar[1], A.Dubolazov[2], A.Pavlyukovich[1], N. Pavlyukovich[1], A.Ushenko[2], A.Motrich[2], M.Gorsky[2], Yu.Tomka[2], V. Zhytaryuk[2]

[1] Bukovinian State Medical University, 3 Theatral Sq., Chernivtsi, Ukraine, 58000
[2] Chernivtsi National University, 2 Kotsiubynskyi Str., Chernivtsi, Ukraine, 58012

a.dubolazov@chnu.edu.ua

ABSTRACT

This section contains the results of a study of the relationships between the 3D distributions of the optical anisotropy parameters of polycrystalline networks of biological fluid films of different biochemical composition and the layered phase sections of volume distributions of the magnitude and parameter phase of the "two-point" Stokes vector of the microscopic image**.**

Keywords: Stokes-correlometry, birefringence, biological tissue, differentiation.

1. INTRODUCTION

In the framework of the statistical approach, using the scale-selective wavelet analysis, the quantities and ranges of statistical 1st-4th order changes that characterize was determine[1-6]:

- distribution of module values and phase parameters of the laser Stokes vector transformed by dendritic and spherulitic polycrystalline networks of films of biological liquids in different phase sections of the object field;
- a set of values of the amplitudes of the wavelet coefficients for different scales of the geometric dimensions of the module maps and the phase of the degree of correlation of the Stokes (DCS) vector parameters.

On this basis, the effectiveness of the 3D Stokes-correlometric mapping of polycrystalline networks in differentiating optically anisotropic urine films of healthy donors and patients with albuminuria is physically justified and experimentally determined.

In order to facilitate the physical analysis of the manifestations of optical anisotropy (distributions of the directions of the optical axes $\rho(r) = arctg\dfrac{E_y(r)}{E_x(r)}$ and phase shifts $\delta(r)$ between the orthogonal components ($E_x(r), E_y(r)$) of the laser wave amplitude) of the biological layers, we rewrite the relation in a slightly different form

$$\begin{cases} S_1 = \mathrm{Re}\, S_1 + \mathrm{Im}\, S_1 = \left[1 + tg\rho_1 tg\rho_2 \cos(\delta_2 - \delta_1)\right] + i\left[tg\rho_1 tg\rho_2 \sin(\delta_2 - \delta_1)\right]; \\ |S_1| = \sqrt{\left[1 + tg^2\rho_1 tg^2\rho_2 + 2tg\rho_1 tg\rho_2 \cos(\delta_2 - \delta_1)\right]}; \\ ArgS_1 = arctg\left[\dfrac{\sin(\delta_2 - \delta_1)}{ctg\rho_1 ctg\rho_2 + \cos(\delta_2 - \delta_1)}\right]. \end{cases} \quad (1)$$

Optics and Photonics for Information Processing XIV, edited by A. A. S. Awwal, K. M. Iftekharuddin, V. H. Diaz-Ramirez, A. Márquez, Proc. of SPIE Vol. 11509, 115090V · © 2020 SPIE
CCC code: 0277-786X/20/$21 · doi: 10.1117/12.2568451

$$\begin{cases} S_2 = \mathrm{Re}\, S_2 + \mathrm{Im}\, S_2 = \left[1 - tg\rho_1 tg\rho_2 \cos(\delta_2 - \delta_1)\right] - i\left[tg\rho_1 tg\rho_2 \sin(\delta_2 - \delta_1)\right]; \\ |S_2| = \sqrt{\left[1 + tg^2\rho_1 tg^2\rho_2 - 2tg\rho_1 tg\rho_2 \cos(\delta_2 - \delta_1)\right]}; \\ ArgS_2 = arctg\left[\dfrac{\sin(\delta_2 - \delta_1)}{ctg\rho_1 ctg\rho_2 - \cos(\delta_2 - \delta_1)}\right]. \end{cases} \quad (2)$$

$$\begin{cases} S_3 = \mathrm{Re}\, S_3 + \mathrm{Im}\, S_3 = \left(\cos\delta_2 + ctg\rho_2 tg\rho_1 \cos\delta_1\right) + i\left(\sin\delta_2 - ctg\rho_2 tg\rho_1 \sin\delta_1\right); \\ |S_3| = \sqrt{\left[1 + ctg^2\rho_2 tg^2\rho_1 - 2ctg\rho_2 tg\rho_1 \cos(\delta_2 - \delta_1)\right]}; \\ ArgS_3 = arctg\left(\dfrac{\sin\delta_2 - ctg\rho_2 tg\rho_1 \sin\delta_1}{\cos\delta_2 + ctg\rho_2 tg\rho_1 \cos\delta_1}\right); \end{cases} \quad (3)$$

$$\begin{cases} S_4 = \mathrm{Re}\, S_4 + \mathrm{Im}\, S_4 = \left(\sin\delta_1 + ctg\rho_2 tg\rho_1 \sin\delta_2\right) + i\left(\cos\delta_1 + ctg\rho_2 tg\rho_1 \cos\delta_2\right); \\ |S_4| = \sqrt{\left[1 + ctg^2\rho_2 tg^2\rho_1 + 2ctg\rho_2 tg\rho_1 \cos(\delta_2 - \delta_1)\right]}; \\ ArgS_4 = arctg\left(\dfrac{\cos\delta_1 + ctg\rho_2 tg\rho_1 \cos\delta_2}{\sin\delta_1 + ctg\rho_2 tg\rho_1 \sin\delta_2}\right). \end{cases} \quad (4)$$

In the future, to simplify (without reducing the completeness of the analysis) we will consider the relation (1) - (4) in the approximation of weak phase modulation ($\delta_i \le 0{,}12$; $\cos(\delta_1 - \delta_2) \to 1$; $\sin(\delta_1 - \delta_2) \to \delta_1 - \delta_2$).

Note that this assumption is not artificial for optically thin histological sections of myocardial tissue and rectal wall. It can be shown that for laser radiation with a wavelength $\lambda = 0.63\mu m$ within the geometric thickness $l = 30\mu m$ of a completely optically anisotropic layer of biological tissue ($\Delta n \approx 10^{-4} \div 1.5 \times 10^{-3}$ [4, 7-10]), the maximum phase shift ($\delta_{12} \equiv \delta = \dfrac{2\pi}{\lambda}\Delta nl$) varies within $0.03 \le \delta \le 0.45$.

Moreover, among birefringent networks or “islands” (clusters of spatially non-oriented protein molecules), there are variations in the transverse sizes of birefringent ($2\mu m \le \Delta l \le 20\mu m$) structures, which form weak phase modulations ($2\mu m \le \Delta\delta \le 20\mu m$) in the plane of the polarization-inhomogeneous image.

Under these conditions, the dependences (1) - (4) take the following form

$$\begin{cases} |S_1| = \left[1 + tg\rho_1 tg\rho_2\right]; \\ ArgS_1 = arctg\left[\dfrac{(\delta_2 - \delta_1)}{1 + ctg\rho_1 ctg\rho_2}\right]. \end{cases} \quad (5)$$

$$\begin{cases} |S_2| = \left[1 - tg\rho_1 tg\rho_2\right]; \\ ArgS_2 = arctg\left[\dfrac{(\delta_2 - \delta_1)}{ctg\rho_1 ctg\rho_2}\right]. \end{cases} \quad (6)$$

$$\begin{cases} |S_3| = 1 - ctg\rho_2 tg\rho_1; \\ ArgS_3 = arctg\left(\dfrac{\delta_2 - \delta_1 ctg\rho_2 tg\rho_1}{1 + ctg\rho_2 tg\rho_1} \right); \end{cases} \quad (7)$$

$$\begin{cases} |S_4| = 1 + ctg\rho_2 tg\rho_1; \\ ArgS_4 = arctg\left(\dfrac{1 + ctg\rho_2 tg\rho_1}{\delta_1 + \delta_2 ctg\rho_2 tg\rho_1} \right). \end{cases} \quad (8)$$

From the analysis of the obtained relations (5) - (7), it follows that the DCS $|S_{i=1;2;3;4}(\Delta x, \Delta y)|$ module carries information on the orientational structure $\rho(x, y)$ of polycrystalline networks and structures. The DCS phase $Arg(S_{i=1;2;3;4}(\Delta x, \Delta y))$ carries information about their birefringence ($\delta(x, y)$).

As is known[12], the first parameter of the Stokes $S_1(r)$ vector characterizes the total intensity at a point r; the second $S_2(r)$ and third $S_3(r)$ are changes in the azimuth and ellipticity of polarization, and the fourth $S_4(r)$ is the magnitude of the ellipticity of polarization. Based on this, in the future we will conduct a detailed analytical and experimental analysis of the polarimetry capabilities of the "two-point" parameters of the Stokes vector using the example $S_3(r_1, r_2)$ of and $S_4(r_1, r_2)$.

2. THE METHODOLOGY FOR MEASURING 3D DISTRIBUTIONS OF THE MODULE AND PHASE OF THE SCS OF THE OBJECT FIELD OF THE BIOLOGICAL LAYER.

A generalization of the polarization interferometry scheme is the scheme of Stokes polarimetric mapping, shown in fig. 1.

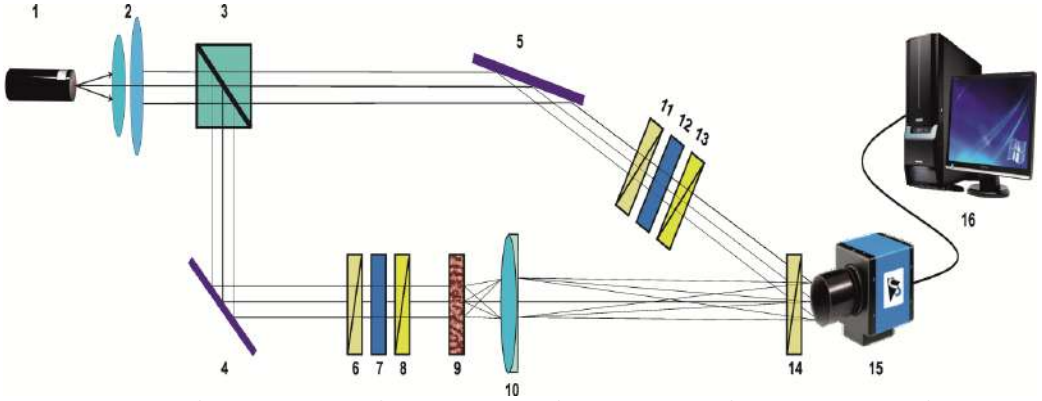

Fig. 1. The optical scheme of polarization-interference mapping of the parameters of the Stokes vector of optically anisotropic biological layers. Explanations in the text.

It is resulted on fig. 1, the optical scheme is supplemented in comparison with the polarization interferometry[12-14] scheme with a polarizer 14, which is located in front of the photosensitive area of the digital camera 15.

The method of polarization-correlation determination of the set of parameters of the Stokes vector consists in the following set of actions:

- The simultaneous formation in the "irradiating" and "reference" parallel laser beams of one of these polarization states (for example $\left(0^0-0^0\right);\ \left(90^0-90^0\right);\ \left(45^0-45^0\right);\ \left(135^0-135^0\right);\ (\otimes-\otimes);\ (\oplus-\oplus)$).

- For each of these polarization states, registration of each partial interference pattern is experimentally carried out through the polarizer-analyzer 14 with the orientation of the transmission plane at angles $\Theta=0^0;\ \ \Theta=90^0$.

- Recovery for each partial polarization-interference distribution in the aggregate of phase cross sections using the integrated diffraction transformation of the coordinate distributions of complex amplitudes of the object field in the plane of the microscopic image of the biological layer.

- Recovery for each partial polarization-interference distribution in the aggregate of phase cross sections $\varphi=const$ using the integrated diffraction transformation of the coordinate distributions of complex amplitudes $\left\{E_x(\varphi,r);\ \ E_y(\varphi,r)\right\}$ of the object field in the plane of the microscopic image of the biological layer.

- Calculation in each phase plane ($\varphi_k=k\Delta\varphi, k=0;1;2;...$) of coordinate distributions (x,y) of a set of Stokes vector parameters $S_{i=1;2;3;4}(\varphi,x,y)$ and polarization parameters $\alpha(\varphi,x,y)$ and $\beta(\varphi,x,y)$ according to the following algorithms

$$\begin{aligned}
S_1(\varphi_k,x,y)&=\left(|E_x|^2+|E_y|^2\right)(\varphi_k,x,y);\\
S_2(\varphi_k,x,y)&=\left(|E_x|^2-|E_y|^2\right)(\varphi_k,x,y);\\
S_3(\varphi_k,x,y)&=2\,\mathrm{Re}\left|E_xE_y^*\right|(\varphi_k,x,y);\\
S_4(\varphi_k,x,y)&=2\,\mathrm{Im}\left|E_xE_y^*\right|(\varphi_k,x,y).
\end{aligned} \tag{9}$$

$$\alpha(\varphi_k,x,y)=0{,}5arctg\left[\frac{S_3(\varphi_k,x,y)}{S_2(\varphi_k,x,y)}\right]; \tag{10}$$

$$\beta(\varphi_k,x,y)=0{,}5arctg\left[\frac{S_4(\varphi_k,x,y)}{S_1(\varphi_k,x,y)}\right]. \tag{11}$$

The experimental technique of Stokes-correlometric mapping of an object field of a biological layer consists in the following sequence of steps:

1. Irradiate sample 6 with a circularly polarized laser light beam 1, which provides a filter that consists of quarter-wave plates 3,5 and a polarizer 4 (fig);

2. Rotate the transmission axis of the polarizer-analyzer 9 (in the absence of a quarter-wave plate 8) by the angles $\Theta=0^0,\ \ \Theta=90^0,\ \ \Theta=45^0,\ \ \ \Theta=135^0$ and measure the intensity of the transmitted radiation $I_0^{\otimes};I_{90}^{\otimes};I_{45}^{\otimes};I_{135}^{\otimes};$

3. The magnitude of the first, second and third parameters of the Stokes vector is calculated within each pixel of the digital camera 11 $S_{i=1;2;3}^{\otimes}$

$$S_1=I_0^{\otimes}+I_{90}^{\otimes}; \tag{12}$$

$$S_2=I_0^{\otimes}-I_{90}^{\otimes}; \tag{13}$$

$$S_3 = I_{45}^{\otimes} - I_{135}^{\otimes}. \tag{14}$$

4. Install a quarter-wave plate 8 in front of the polarizer-analyzer 9, orient its axis of maximum speed at angles $+45^0$ and -45^0 relative to the plane of transmission of the polarizer, and measure the intensity of the transmitted radiation $I_{\otimes}^{\otimes}; I_{\oplus}^{\otimes}$.

5. Calculate a two-dimensional array of values of the fourth parameter of the Stokes vector S_4.

$$S_4 = I_{\otimes}^{\otimes} - I_{\oplus}^{\otimes}. \tag{15}$$

6. Calculate the coordinate distribution of the values of the two-point parameters of the Stokes vector according to the following algorithms:

$$\begin{cases} |S_2| = \sqrt{\left[\sqrt{I_0(r_1)I_0(r_2)} - \sqrt{I_{90}(r_1)I_{90}(r_2)}\cos(\delta_2 - \delta_1)\right]^2 + \left[\sqrt{I_{90}(r_1)I_{90}(r_2)}\sin(\delta_2 - \delta_1)\right]^2}; \\ ArgS_2 = arctg\left(\dfrac{\left[\sqrt{I_{90}(r_1)I_{90}(r_2)}\sin(\delta_2 - \delta_1)\right]}{\left[\sqrt{I_0(r_1)I_0(r_2)} - \sqrt{I_{90}(r_1)I_{90}(r_2)}\cos(\delta_2 - \delta_1)\right]}\right). \end{cases} \tag{16}$$

$$\begin{cases} |S_3| = \sqrt{\left[\sqrt{I_0(r_1)I_{90}(r_2)}\cos\delta_2 + \sqrt{I_0(r_2)I_{90}(r_1)}\cos\delta_1\right]^2 + \\ + \left[\sqrt{I_0(r_1)I_{90}(r_2)}\sin\delta_2 - \sqrt{I_0(r_2)I_{90}(r_1)}\sin\delta_1\right]^2}; \\ ArgS_3 = arctg\left(\dfrac{\left[\sqrt{I_0(r_1)I_{90}(r_2)}\sin\delta_2 - \sqrt{I_0(r_2)I_{90}(r_1)}\sin\delta_1\right]}{\left[\sqrt{I_0(r_1)I_{90}(r_2)}\cos\delta_2 + \sqrt{I_0(r_2)I_{90}(r_1)}\cos\delta_1\right]}\right). \end{cases} \tag{17}$$

$$\begin{cases} |S_4| = \sqrt{\left[\sqrt{I_0(r_2)I_{90}(r_1)}\sin\delta_1 + \sqrt{I_0(r_1)I_{90}(r_2)}\sin\delta_2\right]^2 + \\ + \left[\sqrt{I_0(r_2)I_{90}(r_1)}\cos\delta_2 + \sqrt{I_0(r_1)I_{90}(r_2)}\cos\delta_1\right]^2}; \\ ArgS_4 = arctg\left(\dfrac{\left[\sqrt{I_0(r_2)I_{90}(r_1)}\cos\delta_2 + \sqrt{I_0(r_1)I_{90}(r_2)}\cos\delta_1\right]}{\left[\sqrt{I_0(r_2)I_{90}(r_1)}\sin\delta_1 + \sqrt{I_0(r_1)I_{90}(r_2)}\sin\delta_2\right]}\right). \end{cases} \tag{18}$$

$$\delta(r) = arctg\left[\left(\frac{S_4(r)S_2(r)}{S_3(r)}\right)\left(\frac{1+\dfrac{I_{90}(r)}{I_0(r)}}{1-\dfrac{I_{90}(r)}{I_0(r)}}\right)\right]. \tag{19}$$

Here I_0 and I_{90} - intensities in the orientation of the transmission plane of the polarizer 0^0 and 90^0; δ_i - phase shifts between orthogonal components of the amplitude of the laser radiation at points with coordinates r_1 and r_2.

In the experimental arrangement of the Stokes polarimeter with a reference laser wave (fig. 1), the following sequence of actions:

- Form similar polarization states in the "irradiating" and "reference" parallel laser beams - for example, $(0^0 - 0^0)$; $(90^0 - 90^0)$; $(45^0 - 45^0)$; $(135^0 - 135^0)$; $(\otimes - \otimes)$; $(\oplus - \oplus)$.

- For each of these polarization states, each partial interference pattern through the polarizer-analyzer 14 with the orientation of the transmission plane at angles is recorded $\Theta = 0^0;\quad \Theta = 90^0$.

- Restore the coordinate distributions of the complex amplitudes $\{E_x(\varphi, r);\quad E_y(\varphi, r)\}$ of the object field in the plane of the microscopic image of the biological layer for each partial polarization-interference distribution in the aggregate of phase cross sections $\varphi = const$ using the integral diffraction transformation.

- Calculate (relation (9)) in each phase plane ($\varphi_k = k\Delta\varphi, k = 0;1;2;...$) the coordinate distributions (x, y) of the set of parameters of the Stokes vector $S_{i=1;2;3;4}(\varphi, x, y)$.

- Algorithms (16) - (19) are used to calculate the layered distributions of the modulus $|S_{i=1;2;3;4}|(\varphi, x, y)$ and phase $Arg[S_{i=1;2;3;4}(\varphi, x, y)]$ of the DCS of a polarization-inhomogeneous object field of an optically anisotropic biological layer.

3. 3D DISTRIBUTION OF THE MODULE AND PHASE OF THE "TWO-POINT" STOKES VECTOR OF A MICROSCOPIC IMAGE OF A POLYCRYSTALLINE DENDRITIC NETWORK OF A CEREBROSPINAL FLUID FILM

In this part of the work, we selected the module $|S_4|(\varphi, x, y)$ and phase $ArgS_4(\varphi, x, y)$ of the 4th parameter of the "two-point" Stokes vector, which turned out to be the most sensitive to changes in the optical anisotropy of histological sections of structured and parenchymal biological tissues, as the main information parameter (without reducing the completeness of analysis)

The results of experimental testing of the method of 3D Stokes-correlometric mapping with layer-by-layer digital holographic reproduction of distributions of the magnitude of MDCS ($|S_4|(\varphi, x, y)$ fragments (1), (2)) and PDCS $ArgS_4(\varphi, x, y)$ fragments (3), (4)) of a microscopic image of a polycrystalline cerebrospinal fluid film according to the method described in [] are presented the series of fig. 2 ($\varphi = 0{,}4rad$), fig. 5 ($\varphi = 0{,}8rad$) and fig. 8 ($\varphi = 1{,}2rad$).

In fig. 3, fig. 6, fig. 9 shows the topographic structure (100pix 100pix) of the distribution of the magnitude of the module $|S_4|$ (fragment (1)) and phase $ArgS_4$ (fragment (2)) of the "two-point" 4th parameter of the Stokes vector of the microscopic image of the polycrystalline cerebrospinal fluid film obtained for a series of phase cross sections $\varphi = 0{,}4rad$, $\varphi = 0{,}8rad$ and $\varphi = 1{,}2rad$, respectively

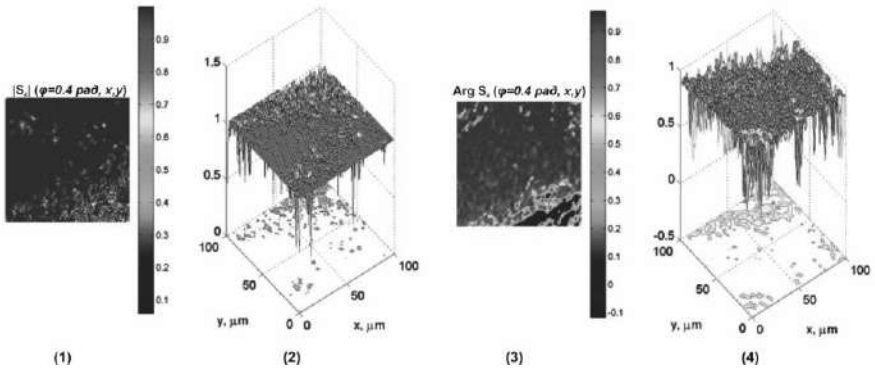

Fig. 2. Distributions of the magnitude of the modulus $|S_4|$ (fragments (1), (2)) and phase $ArgS_4$ (fragments (3), (4)) of the "two-point" 4th parameter of the Stokes vector of the microscopic image of the polycrystalline cerebrospinal fluid film for the phase section $\varphi = 0{,}4$. Explanation in the text.

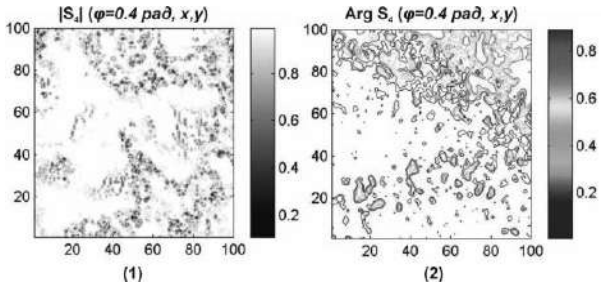

Fig. 3. Maps (100pix 100pix) of the distributions of the magnitude of the module $|S_4|$ (fragment (1)) and phase $ArgS_4$ (fragment (2)) of the "two-point" 4th parameter of the Stokes vector of the microscopic image of the polycrystalline cerebrospinal fluid film for the phase section $\varphi = 0{,}4$. Explanation in the text.

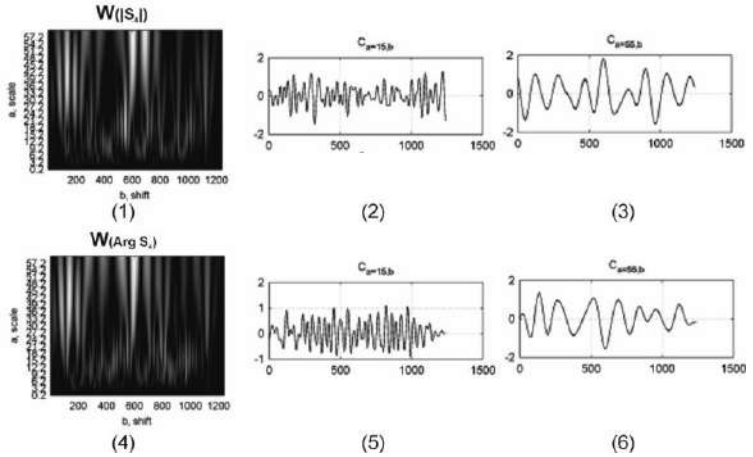

Fig. 4. Maps (fragments (1), (4)) and linear sections (fragments (2), (3), (5), (6)) wavelet coefficients of the distribution of the magnitude of the module $|S_4|$ (fragments (1) - (3)) and phases $ArgS_4$ (fragments (3) - (6)) of the "two-point" 4th parameter of the Stokes vector of the microscopic image of the polycrystalline cerebrospinal fluid film for the phase section $\varphi = 0{,}4$. Explanation in the text.

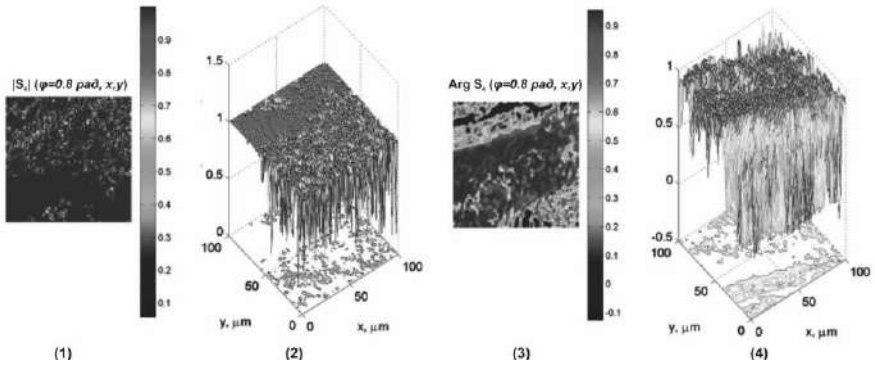

Fig. 5. Distributions of the magnitude of the modulus $|S_4|$ (fragments (1), (2)) and phase $ArgS_4$ (fragments (3), (4)) of the "two-point" 4th parameter of the Stokes vector of the microscopic image of the polycrystalline cerebrospinal fluid film for the phase section $\varphi = 0{,}8$. Explanation in the text.

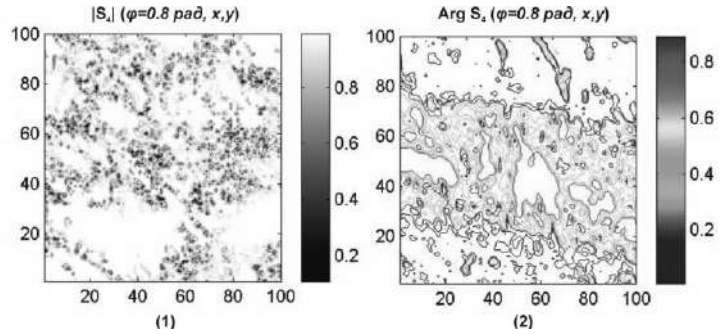

Fig. 6. Maps (100pix 100pix) of the distributions of the magnitude of the module $|S_4|$ (fragment (1)) and phase $ArgS_4$ (fragment (2)) of the "two-point" 4th parameter of the Stokes vector of the microscopic image of the polycrystalline cerebrospinal fluid film for the phase section $\varphi = 0{,}8$. Explanation in the text.

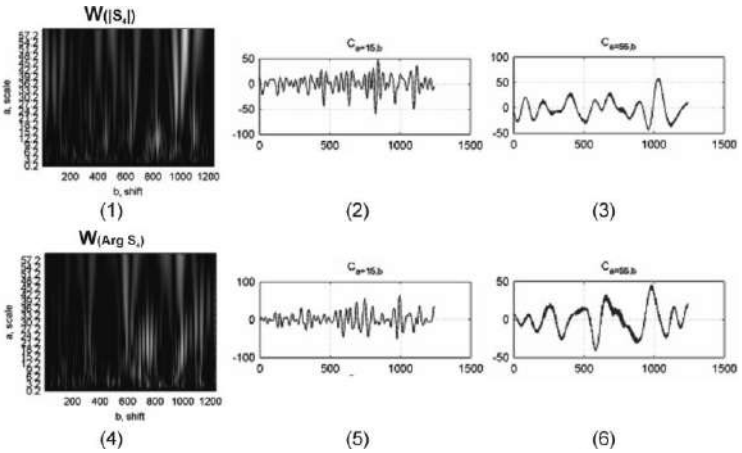

Fig. 7. Maps (fragments (1), (4)) and linear sections (fragments (2), (3), (5), (6)) wavelet coefficients of the distribution of the magnitude of the module $|S_4|$ (fragments (1) - (3)) and phases $ArgS_4$ (fragments (3) - (6)) of the "two-point" 4th parameter of the Stokes vector of the microscopic image of the polycrystalline cerebrospinal fluid film for the phase section $\varphi = 0{,}8$. Explanation in the text.

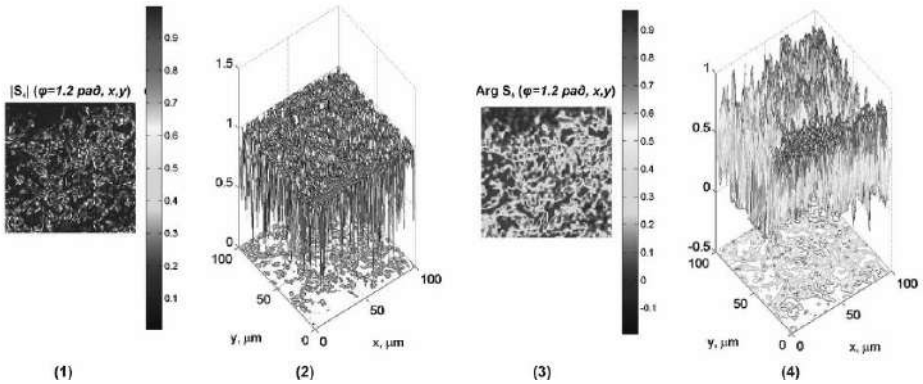

Fig. 8. Distributions of the magnitude of the modulus $|S_4|$ (fragments (1), (2)) and phase $ArgS_4$ (fragments (3), (4)) of the "two-point" 4th parameter of the Stokes vector of the microscopic image of the polycrystalline cerebrospinal fluid film for the phase section $\varphi = 1{,}2$. Explanation in the text.

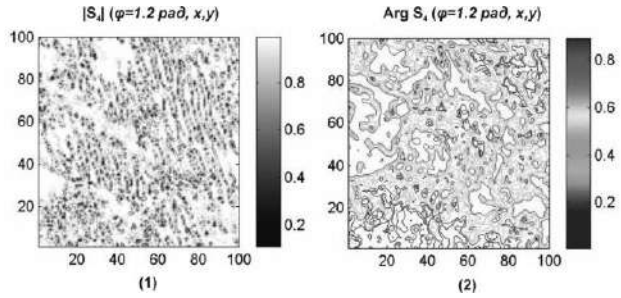

Fig. 9. Maps (100pix 100pix) of the distributions of the magnitude of the module $|S_4|$ (fragment (1)) and phase $ArgS_4$ (fragment (2)) of the "two-point" 4th parameter of the Stokes vector of the microscopic image of the polycrystalline cerebrospinal fluid film for the phase section $\varphi = 1{,}2$. Explanation in the text.

Maps (fragments (1), (4)) and linear sections (fragments (2), (3), (5), (6)) wavelet coefficients of the distribution of the magnitude of the module $|S_4|$ (fragments (1) - (3)) and phases $ArgS_4$ (fragments (3) - (6)) of the "two-point" 4th parameter of the Stokes vector of the microscopic image of a polycrystalline cerebrospinal fluid film are presented in fig. 4 ($\varphi = 0{,}4rad$), fig. 7 ($\varphi = 0{,}8rad$), fig. 10 ($\varphi = 0{,}8rad$).

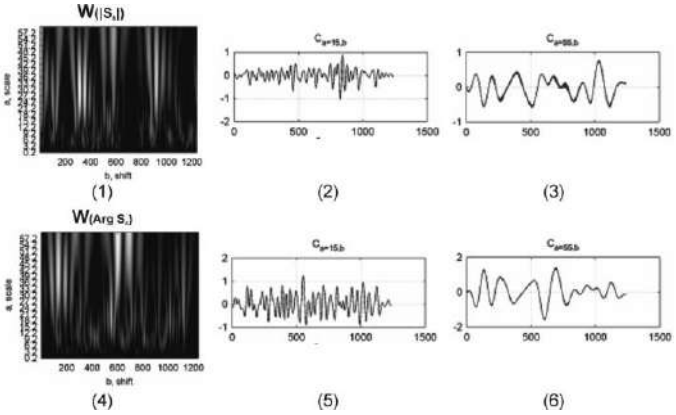

Fig. 10. Maps (fragments (1), (4)) and linear sections (fragments (2), (3), (5), (6)) wavelet coefficients of the distribution of the magnitude of the module $|S_4|$ (fragments (1) - (3)) and phases $ArgS_4$ (fragments (3) - (6)) of the "two-point" 4th parameter of the Stokes vector of the microscopic image of the polycrystalline cerebrospinal fluid film for the phase section $\varphi = 1{,}2$. Explanation in the text.

An analysis of the data obtained by 3D Stokes-correlometric mapping of the object field of laser radiation from a network of dendritic crystals of a cerebrospinal fluid film (fig. 2 - fig. 10) was found:

1. The main polarimetric manifestations of the correlation matching in the directions of the optical axes ($|S_4|$) and birefringence ($ArgS_4$) of the polycrystalline network of the optically anisotropic liquor layer is the formation of the distributions of the MDCS $|S_4|(\varphi, x, y)$ and PDCS $ArgS_4(\varphi, x, y)$ values (fig. 2, fig. 3, fig. 5, fig. 6.5, fig. 8, fig. 9).

2. Each of the coordinate distributions $|S_4|(\varphi, x, y)$ and $ArgS_4(\varphi, x, y)$, within the limits of partial phase cross sections $\varphi_i = 0{,}4rad;\ 0{,}8rad;\ 1{,}2rad$, has an individual statistical (fig. 2, fig. 5, fig. 8) and topographic structure - fig. 3, fig. 6, fig. 9.

3. With increasing ($\uparrow$), the values of the phase section ($\varphi\uparrow$) of the field of complex amplitudes increase the range of changes in the local values of the module $|S_4|(\varphi,x,y)$ and phase $ArgS_4(\varphi,x,y)$ - fig. 3, fig. 6, fig. 9 respectively.

Let us analyze the results obtained from a physical point of view. In the process of crystallization of the cerebrospinal fluid film, various crystalline fractions are formed in its partial layers. Among them, two main, predominant other biochemical compounds in concentration can be distinguished. The first is large-scale ($20\mu m \div 100\mu m$) needle-shaped with spatially oriented directions of the optical axes linearly birefringent albumin crystals (~ 70% - 80%). The second is small-scale ($5\mu m \div 20\mu m$) spherulite globulin crystals (~ 20% - 30%), which are characterized by phase modulation of circularly polarized components of the laser radiation amplitude, or circular birefringence.

Thus, in the planar partial layers of the cerebrospinal fluid film, a predominantly polycrystalline dendritic phase-modulating (δ) network of albumin crystals with randomly located directions (ρ) of optical axes is formed.

Within the framework of model ideas about the formation of the polarization-correlation structure of the object field of a birefringent medium with weak phase fluctuations, the relationships between the module and the DCS phase were determined. In particular, the MDCS is determined by the directions of the optical axes of the needle crystals $|S_4|(r_1,r_2)\leftrightarrow(\rho_1,\rho_2)$, and the PDCS value is associated with the phase modulation of the orthogonal components of the amplitude by optically anisotropic dendritic and spherulite crystals $ArgS_4(r_1,r_2)\leftrightarrow(\delta_1,\delta_2)$. As a result, in each such plane of the polarization-inhomogeneous object field of the polycrystalline cerebrospinal fluid film, an individual coordinate () distribution of the magnitude of the module $|S_4|(x,y)$ and phase $ArgS_4(x,y)$ is formed.

Using the reference wave by applying the digital holographic reconstruction algorithm, it is possible to reproduce in different phase (φ) sections of the distribution of the field of complex amplitudes $E_x(\varphi,x,y)$, $E_x(\varphi,x,y)$. On this basis, layer-by-layer distributions $|S_4|(\varphi,x,y)$ and $ArgS_4(\varphi,x,y)$ of the 4th parameter of the Stokes vector of the object field of the polycrystalline network of the cerebrospinal fluid film are determined.

For small values of the phase cross section $\varphi = 0{,}4rad$, the most probable events are the interaction of laser radiation with individual needle and spherulite crystals. From the point of view of the optical-geometric structure of such a network in a given plane:

- a certain spatial-determined distribution of the orientations of the optical axes with a small dispersion of the variation of their values ($\Delta\rho/\rho\langle 1$) is realized for several directions of crystalline growth. In other words, for neighboring points (r_1 and r_2) in a given plane, the most likely condition is $\rho(r_1)-\rho(r_2)\to 0$. As a result, in the distribution map of the MDCS $|S_4|(\varphi,x,y)$ the set of local Stokes-correlometric domains with extreme values $|S_4|(\varphi,\Delta x,\Delta y)\to 1$ prevails - fig. 2 (fragments (1), (2)), fig. 3 (fragment (1)) .

- a coordinate distribution of phase shifts ($\delta(x,y)$) is formed between linearly (needle-shaped crystals) and circularly (spherulite crystals) orthogonally polarized components of the laser radiation amplitude with a small modulation amplitude $\Delta\delta \approx 0{,}4rad$. As a result, the distribution map of the DCS phase $ArgS_4(\varphi,x,y)$ is predominantly correlation-consistent sections with extreme values $ArgS_4(\varphi,\Delta x,\Delta y)\to 1$, - fig. 2 (fragments (3), (4)), fig. 3 (fragment (2)).

- due to the presence of a certain variation in the values of the orientational $\overline{\rho}\pm\Delta\rho$ and phase $\overline{\delta}\pm\Delta\delta$ components of the polycrystalline network of the liquor film the distribution $|S_4|(\varphi,x,y)$ and $ArgS_4(\varphi,x,y)$ contain ensembles of Stokes-correlometric domains with other and different from extreme valueses $0\le|S_4|(\varphi,\Delta x,\Delta y)\le 1$ and $0\le ArgS_4(\varphi,\Delta x,\Delta y)\le 1$.

Within the framework of the statistical approach to the analysis of the distributions of MDCS maps (fig. 2, fragments (1), (2), fig. 3, fragment (1)) and the PDCS (fig. 6.1, fragments (3), (4), fig. 3, fragment (2)), one should expect a significant advantage of the values of the statistical moments of higher orders (asymmetry and excess) ($Z_{3;4}\left(\left|S_4\right|(\varphi = 0{,}4rad, \text{x}, \text{y})\right); Z_{3;4}\left(ArgS_4(\varphi = 0{,}4rad, \text{x}, \text{y})\right)$) over the average (Z_1) and dispersion (Z_2).

The results of digital holographic reproduction of polarization-correlation maps $\left|S_4\right|(\varphi, x, y)$ and $ArgS_4(\varphi, x, y)$ for large values of phase cross sections ($\varphi = 0{,}8rad;\ \ 1{,}2rad$) of three-dimensional distribution of the field of complex amplitudes of laser radiation correspond to the physical situation, where the probability of the interaction of partial waves with several optically anisotropic crystalline formations of the polycrystalline network of the cerebrospinal fluid increases.

As a result, the influence on the polarization-correlation structure of such an object field of the range of variation in the directions of the optical axes $\Delta\rho(\varphi, x, y)\uparrow$ of birefringent crystals, as well as the depth of phase modulation $\Delta\delta(\varphi, x, y)\uparrow$ increases . Such a transformation of the optical-geometric structure of the polycrystalline component in these layers of the cerebrospinal fluid film appears to increase in the coordinate decorrelation between the values $\rho(\varphi, x, y)$ and $\delta(\varphi, x, y)$, which is optically manifested in the redistribution of the extreme values of the module $\left|S_4\right|(\varphi, x, y) = 1$ and phase $ArgS_4(\varphi, x, y) = 1{,}75rad$ to a wider range of their changes, $0 \le \left|S_4\right|(\varphi, x, y) \le 1$ and $0 \le ArgS_4(\varphi, x, y) \le 1{,}75rad$ - fig. 5, fig. 8. In addition, in these phase sections, the quantity, area, size and range of changes in the modulus $0 \le \left|S_4\right|(\varphi, \Delta x, \Delta y) \le 1$ and phase $0 \le ArgS_4(\varphi, x, y) \le 1{,}75rad$ within the Stokes-correlometric domains grows - fig. 6 and fig. 9.

Quantitatively (within the limits of the statistical analysis of the maps of the module and the DCS phase) this is manifested in opposite trends in the magnitude of the statistical moments of the 1st – 4th orders characterizing the distribution of the magnitude of the module $\left|S_4\right|(\varphi, \text{x}, \text{y})$ and phase $ArgS_4(\varphi, \text{x}, \text{y})$ — the average and dispersion grow $\left\{Z_{1;2}\left(\left|S_4\right|(\varphi, \text{x}, \text{y})\right); Z_{1;2}\left(ArgS_4(\varphi, \text{x}, \text{y})\right)\right\}\uparrow$; statistical moments of higher orders, on the contrary, decrease - $\left\{Z_{3;4}\left(\left|S_4\right|(\varphi, \text{x}, \text{y})\right); Z_{3;4}\left(ArgS_4(\varphi, \text{x}, \text{y})\right)\right\}\downarrow$ - table 1[15].

Table 1. Statistical moments $Z_{i=1;2;3;4}$ that characterize the distribution of magnitude $\left|S_4\right|$ and $ArgS_4$ microscopic image of a polycrystalline cerebrospinal fluid film

$\left\|S_4\right\|$			$ArgS_4$		
$\varphi = 0{,}4$	Z_1	0,54	$\varphi = 0{,}4$	Z_1	0,93
	Z_2	0,09,		Z_2	0,07
	Z_3	0,53		Z_3	0,81
	Z_4	1,47		Z_4	1,79
$\varphi = 0{,}8$	Z_1	0,39	$\varphi = 0{,}8$	Z_1	0,84
	Z_2	0,12		Z_2	0,11
	Z_3	0,44		Z_3	0,73
	Z_4	1,16		Z_4	1,41
$\varphi = 1{,}2$	Z_1	0,21	$\varphi = 1{,}2$	Z_1	0,51
	Z_2	0,15		Z_2	0,13
	Z_3	0,38		Z_3	0,61
	Z_4	0,89		Z_4	1,24

CONCLUSIONS

A comparative analysis of the changes in the statistical moments of the first and fourth orders of magnitude of the 3D distribution of the magnitude $|S_4|$ and $ArgS_4$ the "two-point" fourth parameter of the Stokes vector of the microscopic image of the polycrystalline cerebrospinal fluid film in different phase sections φ of the cerebrospinal fluid film revealed significant differences between them - $\begin{cases} |S_4| \Rightarrow \Delta Z_1(\varphi) = 2{,}7; \Delta Z_2(\varphi) = 2{,}3; \Delta Z_3(\varphi) = 1{,}9; \Delta Z_4(\varphi) = 1{,}7; \\ ArgS_4 \Rightarrow \Delta Z_1(\varphi) = 1{,}8; \Delta Z_2(\varphi) = 1{,}9; \Delta Z_3(\varphi) = 1{,}3; \Delta Z_4(\varphi) = 1{,}4; \end{cases}$

As can be seen, the statistical moments of the 1st and 2nd orders characterizing the distribution of the magnitude of the module $|S_4|(\varphi, x, y)$ ($Z_{1;2}$ - the differences for different phase cross sections are 2.3- 2.7 times) and phases $ArgS_4(\varphi, x, y)$ ($Z_{1;2}$ - differences for different phase cross sections are 1.8 - 1.9 times) of the polarization-inhomogeneous object field of laser radiation turned out to be the most sensitive to changes in the parameters of linear birefringence (ρ, δ) of the aggregates of the polycrystalline network of dendritic crystals in the volume of the cerebrospinal fluid film.

REFERENCES

[1] Mahalakshmi V, Gururaj N, Sathya R, Sabarinath T, Sivapathasundharam B, Kalaiselvan S. Assessment of histological changes in antemortem gingival tissues fixed at various time intervals: A method of estimation of postmortem interval. Journal of forensic dental sciences. 2016;8(2):114.

[2] Morikawa K, Hyodoh H, Matoba K, Mizuo K, Okazaki S, Watanabe S. Time-related change evaluation of the cerebrospinal fluid using postmortem CT. Legal Medicine. 2016;22:30-5.

[3] Pittner S, Monticelli FC, Pfisterer A, Zissler A, Sanger AM, Stoiber W, et al. Postmortem degradation of skeletal muscle proteins: a novel approach to determine the time since death. Int J Legal Med. 2016;130(2):421-31. 10.1007/s00414-015-1210-6.

[4] Ermida C, Navega D, Cunha E. Luminol chemiluminescence: contribution to postmortem interval determination of skeletonized remains in Portuguese forensic context. International Journal of Legal Medicine. 2017:1-5.

[5] Lu S. Interpretation of Mueller matrices based on polar decomposition / S. Lu, R. A. Chipman // J. Opt. Soc. Am. A. –1996. – Vol. 13. – P.1106-1113.

[6] Ghosh Nirmalya. Techniques for fast and sensitive measurements of two-dimensional birefringence distributions / Nirmalya Ghosh, I. Alex Vitkin // Journal of Biomedical Optics. – 2011. – № 16(11). – P. 110801.

[7] Angelsky, O. V., Bekshaev, A. Y. A., Maksimyak, P. P., Maksimyak, A. P., & Hanson, S. G. (2018). Low-temperature laser-stimulated controllable generation of micro-bubbles in a water suspension of absorptive colloid particles. Optics Express, 26(11), 13995-14009.

[8] Angelsky, O. V. (2007). Optical correlation techniques and applications. Optical correlation techniques and applications (pp. 1-270)

[9] Angelsky, O. V., Ushenko, A. G., Pishak, V. P., Burkovets, D. N., Yermolenko, S. B., Pishak, O. V., & Ushenko, Y. A. (2000). Coherent introscopy of phase-inhomogeneous surfaces and layers. Paper presented at the Proceedings of SPIE - the International Society for Optical Engineering, 4016 413-418.

[10] Angelsky OV, Bekshaev AY, Hanson SG, Zenkova CY, Mokhun II and Jun Z (2020) Structured Light: Ideas and Concepts. Front. Phys. 8:114.

[11] Angelsky OV, Zenkova CY, Hanson SG and Zheng J (2020) Extraordinary Manifestation of Evanescent Wave in Biomedical Application. Front. Phys. 8:159.

[12] Ushenko, Yu.A., Bachynsky, V.T., Vanchulyak, O.Ya., Dubolazov, A.V., Garazdyuk, M.S., Ushenko, V.A., "Jones-matrix mapping of complex degree of mutual anisotropy of birefringent protein networks during the differentiation of myocardium necrotic changes," (2016) Applied Optics, 55 (12), pp. B113-B119.

[13] Ushenko, Yu.A., Dubolazov, A.V., Karachevtcev, A.O., Zabolotna, N.I., "A fractal and statistic analysis of Mueller-matrix images of phase inhomogeneous layers,"(2011) Proceedings of SPIE - The International Society for Optical Engineering, 8134, 81340P.

[14] Ushenko, V.A., Dubolazov, A.V., "Correlation and self similarity structure of polycrystalline network biological layers Mueller matrices images," (2013) Proceedings of SPIE - The International Society for Optical Engineering, 8856.

[15] "Cassidy, "Basic concepts of statistical analysis for surgical research," Journal of Surgical Research 128,199-206 (2005).